Biomass and Bioenergy 201 (2025) 108143

Contents lists available at ScienceDirect

Biomass and Bioenergy

journal homepage: www.elsevier.com/locate/biombioe

# Microwave-assisted hydrothermal carbonization of sago (*Metroxylon* spp) to hydrochar as potential catalyst for etherification of glycerol

Jakaria Rambli [a], Armando T. Quitain [b,c,*], Ramin Khezri [d], Wan Azlina Wan Ab Karim Ghani [e], Suttichai Assabumrungrat [c,f], Tetsuya Kida [c,g]

[a] Department of Materials Science and Applied Chemistry, Graduate School of Science and Technology, Kumamoto University, Kumamoto, 860-8555, Japan
[b] Graduate School of Social and Cultural Sciences, Kumamoto University, Kumamoto, 860-8555, Japan
[c] International Research Organization for Advanced Science and Technology, Kumamoto University, Kumamoto, 860-8555, Japan
[d] Department of Chemical Engineering, Faculty of Engineering, Chulalongkorn University, Bangkok, 10330, Thailand
[e] Department of Chemical & Environmental Engineering/Sustainable Process Engineering Research Centre, Faculty of Engineering, University Putra Malaysia, 43400 UPM, Serdang, Selangor, Malaysia
[f] Bio-Circular-Green-economy Technology & Engineering Center (BCGeTEC) and Center of Excellence in Catalysis and Catalytic Reaction Engineering, Department of Chemical Engineering, Faculty of Engineering, Chulalongkorn University, Bangkok, 10330, Thailand
[g] Faculty of Advanced Science and Technology, Kumamoto University, Kumamoto, 860-8555, Japan

ARTICLE INFO

*Keywords:*
Microwave-assisted
Hydrothermal carbonization
Sago
Hydrochar
Glycerol
GTBE

ABSTRACT

The sustainable management of agricultural waste is crucial for achieving global carbon neutrality. Sago (*Metroxylon* spp) waste is generated in large quantities during starch extraction and is often discarded improperly or burned openly, which leads to significant environmental degradation. In this study, we converted sago waste into valuable hydrochar through microwave-assisted hydrothermal carbonization at temperatures between 200 and 250 °C for 1 h. Proximate and ultimate analyses were performed, as well as analyses of bulk density, pH, thermogravimetric and surface, and structure using scanning electron microscopy and BET. Hydrochar produced at 200 °C had a higher yield (29.8 %) than that produced using conventional heating methods. It also had an enhanced fixed carbon content (22.1–26.4 % compared to 11.04 % in raw biomass) and reduced O/C (0.999–1.432) and H/C (0.007–0.117) ratios. This indicates improved carbonization and hydrophobicity. The BET surface area of the hydrochar increased with temperature, ranging from 57.9 to 179.8 $m^2/g$, with the highest value being reached at 250 °C. SEM analysis revealed that lower temperatures preserved more of the original fibrous structure of the biomass, whereas higher temperatures resulted in greater porosity and surface roughness due to the progressive breakdown and reformation of biomass components. Fourier transform infrared analysis revealed that polar functional groups, such as hydroxyl, carboxyl and carbonyl, decreased at 200 °C, thereby enhancing the stability of the hydrochar. Microwave-assisted hydrothermal carbonization at 200 °C produced hydrochar with balanced properties, achieving 99 % glycerol conversion and 59.9 % glycerol *tert*-butyl ether selectivity, thereby outperforming commercial resin catalysts.

## 1. Introduction

Located near the equator, Malaysia focuses on the agricultural sector as the cornerstone of its economic growth. This results in the production of around 500 million tonnes of crop residue each year [1]. While some of this biomass is repurposed for various applications, around 60–70 % of sago residue is still burned openly to prepare land for subsequent planting cycles [2]. This practice, which is driven by labor shortages and the difficulty of managing multi-cropping systems, contributes significantly to environmental degradation [3]. Each year, burning crop waste in open areas emits around 1.2 Tg (Tg) of particulate matter and 1.8 Tg of greenhouse gases, including $CO_2$, $CH_4$, and $NO_x$, [4,5]. This also elevates soil surface temperatures from 33.8 to 44.2 °C, reducing organic matter and beneficial microbial activity in the topsoil [6].

To address these issues, microwave hydrothermal carbonization (MWHTC) provides an effective thermochemical process for converting

This article is part of a special issue entitled: Biorefineries and Separations published in Biomass and Bioenergy.

* Corresponding author. Graduate School of Social and Cultural Sciences, Kumamoto University, Kumamoto 860-8555, Japan.
*E-mail address:* quitain@kumamoto-u.ac.jp (A.T. Quitain).

https://doi.org/10.1016/j.biombioe.2025.108143
Received 20 May 2025; Received in revised form 26 June 2025; Accepted 27 June 2025
Available online 30 June 2025

raw biomass into energy-rich hydrochar. Compared to traditional pyrolysis and incineration, MWHTC operates at lower temperatures (180–250 °C) and pressures of 10–15 bar (1.0–1.5 MPa) of $CO_2$, significantly reducing energy consumption and emissions [7]. Unlike incineration, which completely combusts biomass and contributes to air pollution, MWHTC retains carbon in the form of hydrochar, which can be used as a solid fuel or catalyst support [8–10].

Although the potential of MWHTC is widely recognized, further optimization is required. Future studies should examine variables such as microwave power, reaction time, feedstock concentration, and the use of additives to enhance hydrochar yield and properties. Hydrochar is an important component of sustainable biomass management due to its high porosity and carbon content, which make it effective for soil amendment, pollutant adsorption, and carbon sequestration [11–17].

The sago palm (*Metroxylon* spp), which produces an estimated 60 million tonnes of biomass annually for the food industry, is a promising yet underutilized feedstock for hydrochar production [18,19]. Using sago waste offers a cost-effective approach and reduces the environmental harm associated with conventional disposal methods [20]. Previous studies have primarily focused on converting sago biomass into biochar via slow pyrolysis and conventional thermal processes. These studies have reported moderate fixed carbon content and limited surface area development [21,22]. For example, the pyrolysis of sago bark and residue at temperatures between 300 and 500 °C has been shown to yield biochar with fixed carbon contents ranging from 18 to 24 %, and with surface areas below 100 $m^2/g$. However, there is limited research on producing hydrochar from sago, particularly using microwave-assisted hydrothermal carbonization methods. Studies evaluating the physicochemical properties and catalytic potential of sago-derived hydrochar generated via MWHTC are scarce to date, highlighting the novelty and significance of the present work.

In addition, the rapid growth of the biodiesel industry has led to an oversupply of crude glycerol, a by-product accounting for around 10 % of biodiesel production. This has led to market saturation and a significant drop in glycerol's commercial value, prompting extensive research into its valorization through chemical conversion into fuel additives and other high-value chemicals [23–25]. One promising approach is the etherification of glycerol to produce glycerol *tert*-butyl ethers (GTBE), which are recognized for their ability to improve fuel properties such as combustion efficiency and reduce particulate emissions when blended with gasoline or diesel. Di- and tri-*tert*-butyl glycerol ethers, in particular, are highly valued due to their high energy density and fuel compatibility.

Traditionally, glycerol etherification has been catalyzed using acidic ion-exchange resins such as Amberlyst-15 and heteropolyacids. While effective, these catalysts have limitations, including low thermal stability, deactivation in aqueous environments, and difficulties in regeneration and reuse. These limitations have led to increased interest in developing green, thermally stable, and reusable solid acid catalysts derived from biomass.

Combination sago-derived hydrochar and glycerol conversion offers a novel, dual-purpose method of addressing agro-industrial waste and promoting sustainable fuel production. This study utilizes sago waste, an under-explored biomass, as a precursor for hydrochar synthesis under low-temperature, microwave-assisted hydrothermal conditions at 200 °C. This offers an energy-efficient, environmentally friendly method. The resulting hydrochar is then used as a carbon-based catalyst to selectively convert glycerol into GTBE (a valuable bio-additive for cleaner fuels). This work introduces a new use for sago waste and crude glycerol, and demonstrates high catalytic performance under mild conditions. This contributes to waste valorization, green chemistry, and circular economy initiatives.

## 2. Materials and methods

### 2.1. Initial treatment procedures for sago material

Sago, harvested in Sarawak, Malaysia, was thoroughly washed with demineralized water before further processing. It was then cut into small pieces of 8–13 cm to allow for better sun exposure during a one-week drying process. The dried biomass was pulverized to a particle size of 1.0–4.0 mm before use. Subsequently, some of the raw material was dried to powder form for subsequent proximate characterization and assessment of physicochemical properties and morphology.

### 2.2. Preparation of hydrochar

The hydrochars were prepared using two hydrothermal treatment methods, using conventional heating and microwave, as described in the following subsections and as shown in the schematic diagram in Fig. 1. The hydrochars produced from sago by the hydrothermal process are labelled SH200, SH250, and SH300, representing those produced at temperatures of 200, 250, and 300 °C, respectively. The hydrochars produced from sago by microwave hydrothermal treatment are labelled M − H 200 and M − H 250, corresponding to those produced at 200 °C and 250 °C, respectively. Several criteria were investigated to determine how the hydrothermal carbonization process affects the morphological, chemical, and functional properties of the hydrochar.

#### 2.2.1. Conventional hydrothermal treatment

Conventional hydrothermal carbonization (HTC) was performed using a custom-made, screw-cap stainless steel reactor capable of withstanding pressures up to 30 bar with an internal volume of approximately 30 mL. The reactor was designed to withstand elevated pressure (up to 30 bar) and was heated during conventional hydrothermal treatment to reach the target temperatures over a period of 1 h. Since temperature has a significant effect on the properties of hydrochar, the procedure was carried out at 200, 250, and 300 °C [26]. To ensure optimal reaction conditions, for each experimental procedure, 0.3 g of the sago biomass was thoroughly mixed with 15 mL of water to initiate the reaction process, filling half of the reactor vessel (initial volume 30 mL). The sealed reactor was then heated at the target temperature for a residence time of 60 min. Upon completion, the samples were cooled to room temperature, and then the hydrochar samples were repeatedly washed, filtered, and dried in an oven set at 105 °C for 24 h to remove residual moisture. Each experiment included three duplicates, and the average results were reported.

#### 2.2.2. Microwave hydrothermal treatment

The dried sago biomass was subjected to hydrothermal carbonization using a MARS 6 system (CEM Corporation) with an EasyPrep vessel. The process was carried out at 200 °C and 250 °C, with temperature as the only variable. In each experiment, a combination of 1 g of biomass and 50 mL of water was heated at 15 °C per minute for 1 h to achieve the desired conditions. After sealing the vessel and stirring the samples until the reaction temperature was reached, the hydrochar was cooled, collected, and dried at 105 °C for 24 h. To ensure consistency, the average result of the three replicate experiments was reported.

### 2.3. Biomass and hydrochar sample characterization

This section describes the characterization methods used to evaluate the effect of hydrothermal carbonization (HTC) temperature on the morphological, chemical, and functional properties of hydrochar derived from sago biomass.

#### 2.3.1. Proximate analysis

The characterization of the biomass and hydrochar samples was evaluated using comprehensive standards methods from the American

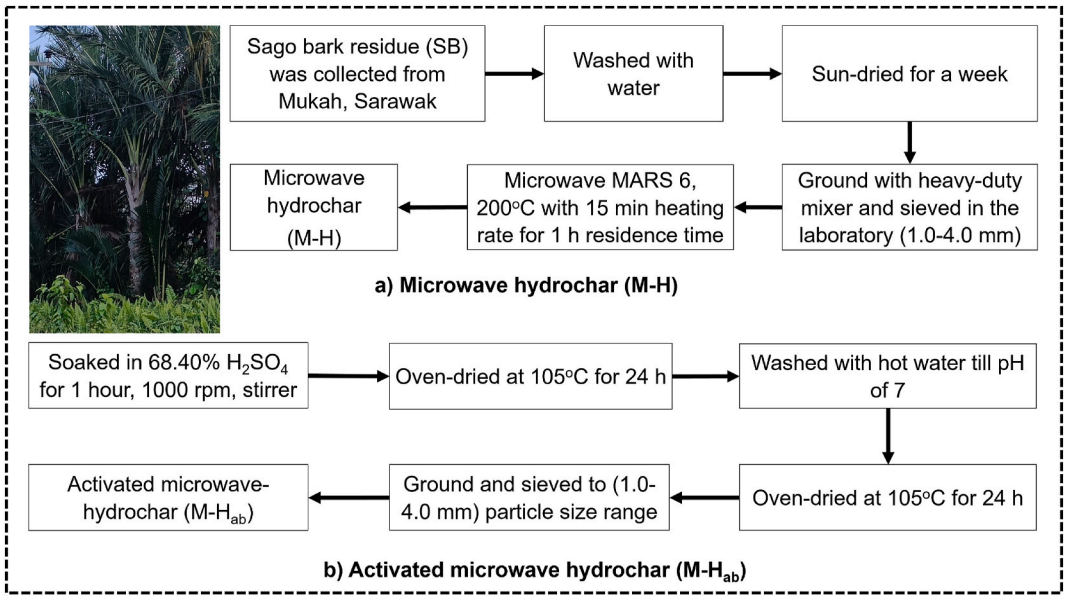


**Fig. 1.** Schematic diagram for the conversion of sago bark to hydrochar.

Society for Testing and Materials (ASTM) [27]. The evaluation used a simultaneous thermogravimetry and differential thermal analysis system (TG/DTA6300, SII NanoTechnology Inc. Japan) to investigate the different components obtained in the samples.

The characterization approach involved several steps. First, the samples were dried in an oven at 105 °C for 2 h to determine the moisture content. The samples were then reheated in a muffle furnace at 950 °C for 7 min to test for volatile elements.

Biomass and hydrochar samples were then heated at 750 °C for 6 h to assess the ash concentration and determine the fixed carbon content. Meanwhile, total ash was determined by subtracting the combined percentages of moisture and volatiles from the total mass. This systematic approach provided a comprehensive breakdown of the characteristics of the biomass and hydrochar, which is essential for understanding their energy potential and composition.

### 2.3.2. Ultimate analysis

The elemental composition of the hydrochar, the contents of sulfur (S), nitrogen (N), hydrogen (H), and carbon (C) were measured using a Micro corder (JM10, J-Science Lab Co., Ltd., Japan). The oxygen content was approximated by the difference, depending on the remaining percentage.

### 2.3.3. Bulk density

Bulk density was determined using a method described in previous studies [28]. Hydrochar powder was added to a graduated cylinder to a specific volume and dried overnight at 80 °C. At the end of the drying process, the cylinder was tapped for 1–2 min to compress the hydrochar, and the bulk density ($m^3/g$) was calculated and recorded.

### 2.3.4. pH measurement

The pH of the biomass and hydrochar samples was measured by mixing 1 g of the sample with deionized water in a 100 mL beaker. The solution was then shaken in a shaker at 220 rpm for 1 h at room temperature. A portable digital pH meter was used to measure the pH of the biomass and hydrochar samples. All experiments were carried out in triplicate and mean values with standard deviation are presented.

### 2.3.5. Morphological and surface analysis

Field-Emission Scanning Electron Microscopy (FESEM, JEOL Ltd., Japan) was used to characterise the surface morphology of the hydrochar, and the surface area was measured using a BET analyzer (BEL MicrotracBEL Corp., Belsorp Max, Japan). The samples were dried and degassed before analysis. X-ray diffraction (XRD) using Cu Kα radiation ($_{\lambda} = 0.154$ nm) on a MiniFlex600 instrument was used to assess crystallinity. The scan angle ranged from 5° to 90°.

### 2.3.6. Post-treatment and catalyst preparation

HTC hydrochar that had been post-treated (washed with deionized water, filtered, and dried at 105 °C for 24 h after cooling) was used for the subsequent process. The microwave-assisted hydrochar (M − H) was then chemically activated by immersion in 68.40 % $H_2SO_4$ with stirring at 1000 rpm. The hydrochar was then washed several times with distilled water until the pH stabilized around neutral (approximately pH 7). Finally, the modified hydrochar (M-$H_{ab}$) was dried at 105 °C for a further 24 h, sieved to a particle size of 1.0–4.0 mm, and stored for further use.

## 2.4. Synthesis of GTBE using sago hydrochar as a catalyst

Reagent-grade glycerol (99 %) and *tert*-butyl alcohol (99.85 % purity, TBA) were used for the etherification analysis (Fujifilm Wako Pure Chemical Co., Japan). The reactions were conducted under controlled conditions at a temperature of 110 °C using microwave irradiation. During each experiment, the mixture was continuously stirred while the temperature was gradually increased to the target set point. A built-in pressure sensor was used to monitor system pressure throughout the reaction. In a typical run, 0.3 g of glycerol was mixed with *tert*-butyl alcohol at a molar ratio of 1:4 (glycerol:TBA). The catalyst was added at 5 % relative to the glycerol mass, and the reaction was maintained at 110 °C for 60 min. After completion, the mixture was cooled to below 50 °C, filtered, and the resulting liquid product was collected for analysis. To investigate the influence of reagent concentration on catalytic performance, further glycerol etherification reactions were carried out using three different TBA:glycerol molar ratios (4:1, 6:1, and 8:1), while keeping all other parameters constant. This enabled the effect of increasing TBA concentration on conversion and GTBE selectivity to be evaluated.

### 2.4.1. Control experiment

In order to assess the catalytic efficiency of the sago hydrochar, a control experiment was carried out without any catalyst under identical

conditions. This baseline test showed no significant etherification, confirming that the conversion of glycerol and TBA was catalyzed solely by the hydrochar.

#### 2.4.2. Reusability and stability of the catalyst

The reusability of the sago hydrochar catalyst was evaluated through multiple reaction cycles under consistent operating conditions. The same amount of catalyst was used for each cycle. After each reaction, the catalyst was recovered by filtration and washed several times, first with methanol and then with distilled water, to remove any adsorbed organic or polar residues. The cleaned catalyst was then dried in an oven at 105 °C for 24 h before being reused in the next reaction cycle. The reproducibility of the results was confirmed by conducting each experiment in triplicate. The performance observed over repeated cycles provided valuable insights into the catalyst's stability, retention of activity, and long-term usability in the synthesis of GTBE.

### 2.5. Product identification by gas chromatography-mass spectrometry (GC-MS)

The final supernatant was then collected for further analysis. The resulting supernatant was diluted with methanol, which acts as an organic solvent. A 1.5 μL sample of the solution was analyzed by gas chromatography for both quantitative and qualitative assessment. Product composition was determined using a GC-MS system (GCMS-QP2010 SE, Shimadzu Corporation, Japan) coupled to an Agilent J&W HP-5ms capillary column (30 m × 0.25 mm ID x 0.25 μm film thickness), with a 5 min temperature ramp to 240 °C.

#### 2.5.1. Product selectivity and glycerol conversion rate calculations

The calculation of Glycerol conversion rate ($X_{Gly}$) and product selectivity (S) is according to Ref. [29]:

$$X_{Gly}(\%) = \frac{V_{GTBE}}{V_{Gly,0}} \times 100 \quad (1)$$

$$S_i(\%) = \frac{V_i}{V_{GTBE}} \times 100 \quad (2)$$

Where $V_{GTBE}$ is the total volume (mmol) of GTBE products, $V_{Gly,0}$ is the initial glycerol volume (mmol), and $V_i$ is the volume of compound i.

The peak area represents the concentration of each component, determined using the corresponding calibration data. Mono-*tert*-butyl glycerol ether (MTBG) exists as two isomers (MTBG 1 and MTBG 2) with similar chemical structures, and both were quantified using the same calibration curve. MTBG is a primary etherification product formed by the substitution of one hydroxyl group on glycerol with a *tert*-butyl group. Di-*tert*-butyl glycerol ether (DTBG) and tri-*tert*-butyl glycerol ether (TTBG) are higher-order etherification products where two or three hydroxyl groups are replaced with *tert*-butyl groups, respectively. The response factors for DTBG and TTBG were calculated relative to MTBG, based on their proportional peak areas and retention characteristics [30]. Glycerol is positioned as a reaction conversion signal when excess TBA is present, ensuring its availability throughout all reaction steps.

The following is the definition of glycerol conversion [31]:

$$X_{Gly}(\%) = \frac{(MTBGs + DTBGs + TTBG)mmol/L}{(Glycerol\,remaining + MTBGs + DTBGs + TTBG)mmol/L} X\,100 \quad (3)$$

At the end of the reaction, the sago hydrochar catalyst was recovered, washed with ethanol and distilled water, and then dried at 105 °C for 24 h. It was then tested using the same procedure as above. To assess the reusability of the solid, multiple reactions were carried out under identical conditions with the same amount of sago hydrochar catalyst to ensure an adequate catalyst supply for subsequent runs, with a minimum of three replicates.

## 3. Results and discussion

The experimental setup for this investigation was designed best on theoretical principles and previous empirical studies of hydrothermal carbonization (HTC), paying particular attention to microwave-assisted HTC (MWHTC) [32]. These parameters were tuned to maximize hydrochar yield and improve catalytic performance. The results obtained are consistent with those reported by Refs. [33,34], who demonstrated the effectiveness of MWHTC in improving the physical and chemical properties of biomass-derived hydrochars.

### 3.1. Physical and compositional properties of microwave-assisted vs. conventional

Table 1 presents the preliminary and final analytical results of the sago biomass and the corresponding hydrochars produced via conventional (SH-Conv) and microwave-assisted hydrothermal carbonization (M − H). In comparison to SH-Conv, microwave-assisted carbonization produced hydrochars with lower moisture and volatile matter contents and higher fixed carbon contents. At 250 °C, SH-Conv hydrochar had a volatile content of 79.40 %, slightly higher than that produced at 200 °C (76.40 %). In contrast, M − H at 200 °C resulted in a lower volatile fraction, indicating more efficient carbonization under microwave irradiation. When comparing the two carbonization methods, the fixed carbon content increased significantly at 250 °C, rising from 11.30 % in hydrochar produced by conventional hydrothermal carbonization (SH-Conv) to 26.42 % in hydrochar produced by microwave-assisted hydrothermal carbonization (M − H). This is consistent with trends reported in previous studies [35]. These data indicate that both methods support increasing carbon densification with temperature, although the microwave method achieves more effective degassing at lower energy input.

Ash mass fractions increasing temperature, from 1.20 % (SH 200 °C) to 2.40 % (SH 250 °C), consistent with the accumulation of thermally resistant inorganic residues [35,36]. While ash can facilitate certain hydrothermal reactions, high ash content is detrimental to fuel applications due to its negative impact on energy density and potential transportation issues [37]. At identical temperatures, the M − H process produced less ash than SH-Conv, making it more suitable for energy and soil amendment applications.

The hydrochar yield of M − H decreased slightly from 29.80 % to 27.10 % as the temperature increased from 200 °C to 250 °C, reflecting greater devolatilization. Contrary to the previously mentioned trend, the yield of hydrochar produced by conventional hydrothermal carbonization (SH-Conv) increased slightly with temperature. It rose from 12.76 % at 200 °C to 13.05 % at 250 °C and reached 14.00 % at 300 °C. Microwave heating promotes a rapid internal temperature rise, which improves carbonization efficiency while preserving biomass structure [34,38].

Microwave-assisted hydrochars exhibited significantly higher carbon content (53.55 % at 200 °C) than SH-Conv samples (46.34 % at 200 °C), accompanied by lower hydrogen and oxygen contents. These trends reflect the dominance of dehydration and decarboxylation reactions accelerated by microwave energy, which increases carbon densification and surface polarity through the loss of -OH and COOH functional groups [39]. A significant decrease in oxygen content, particularly in M − H 250 (41.93 %), reinforces the superior deoxygenation capability of microwave-assisted processes. The hydrogen content decreased from 6.67 % in the raw sago to 4.13 % after the M − H process.

Elemental analysis revealed that the hydrochar produced by microwave-assisted hydrothermal carbonization at 200 °C (M − H 200) had the lowest O/C (0.783) and the lowest H/C ratio (0.007). This indicates a high degree of carbonization, deoxygenation, and aromaticity,

**Table 1**
Elemental composition (CHNS, O), moisture, volatiles, ash, and fixed carbon content of hydrochar produced at different HTC temperatures.

| Compounds | Sago biomass | M – H 200 | M – H 250 | SH-Conv 200 | SH-Conv 250 | SH-Conv 300 |
|---|---|---|---|---|---|---|
| Hydrochar Yield | – | 29.80 ± 0.18 | 27.10 ± 0.11 | 12.76 ± 0.17 | 13.05 ± 0.18 | 14.00 ± 0.10 |
| Moisture | 10.74 ± 0.13 | 10.00 ± 0.03 | 9.58 ± 0.20 | 9.48 ± 0.18 | 6.90 ± 0.10 | 13.00 ± 0.10 |
| Volatile Matter (VM)[a] | 74.58 ± 0.20 | 66.90 ± 0.17 | 63.00 ± 0.10 | 76.40 ± 0.14 | 79.40 ± 0.04 | 65.80 ± 0.18 |
| Ash[a] | 3.64 ± 0.10 | 1.00 ± 0.05 | 1.00 ± 0.03 | 1.20 ± 0.12 | 2.40 ± 0.11 | 1.00 ± 0.05 |
| Fixed Carbon (FC)[a,c] | 11.04 ± 0.25 | 22.10 ± 0.31 | 26.42 ± 0.20 | 12.92 ± 0.11 | 11.30 ± 0.20 | 20.20 ± 0.10 |
| Carbon[b] | 37.21 ± 0.17 | 53.55 ± 0.19 | 38.54 ± 0.11 | 46.34 ± 0.13 | 47.34 ± 0.17 | 47.55 ± 0.15 |
| Hydrogen[b] | 6.67 ± 0.18 | 4.13 ± 0.13 | 5.92 ± 0.18 | 5.42 ± 0.13 | 5.01 ± 0.03 | 3.21 ± 0.03 |
| Nitrogen[b] | 0.20 ± 0.39 | 0.23 ± 0.01 | 0.19 ± 0.20 | 0.18 ± 0.15 | 0.19 ± 0.02 | 0.21 ± 0.04 |
| Sulfur[b] | 0.19 ± 0.32 | 0.16 ± 0.18 | 0.13 ± 0.25 | 0.15 ± 0.18 | 0.13 ± 0.12 | 0.15 ± 0.18 |
| Oxygen[c] | 55.73 ± 0.12 | 41.93 ± 0.03 | 55.22 ± 0.03 | 47.91 ± 0.19 | 47.33 ± 0.13 | 48.88 ± 0.18 |
| H/C (ar) | – | 0.007 ± 0.13 | 0.015 ± 0.20 | 0.117 ± 0.19 | 0.106 ± 0.13 | 0.067 ± 0.15 |
| O/C (ar) | – | 0.783 ± 0.20 | 1.432 ± 0.30 | 1.034 ± 0.12 | 0.999 ± 0.18 | 1.028 ± 0.14 |
| HHV (MJ/kg) | 22.16 ± 0.11 | 23.88 ± 0.18 | 22.52 ± 0.11 | 19.48 ± 0.18 | 19.80 ± 0.16 | 20.03 ± 0.11 |

C represents carbon, H denotes hydrogen, N indicates nitrogen, O stands for oxygen, and S refers to sulfur.
ar: Atomic ratio.
M-H: Microwave hydrochar; SH-Conv: Sago hydrochar – Conventional heating.
[a] Percentage of dry matter representing the results.
[b] Percentage of dry matter devoid of ashes.
[c] Determined by difference.

all of which contribute to enhanced fuel quality. By contrast, the hydrochar produced at 250 °C via microwave-assisted hydrothermal carbonization (M – H 250) had the highest O/C ratio (1.432) and lowest H/C ratio (0.015) among all the conditions tested, suggesting incomplete dehydration alongside significant aromatic condensation [40].

The nitrogen content of the hydrochars was generally higher than that of the raw sago biomass, likely due to protein hydrolysis and nitrogen retention during hydrothermal treatment, consistent with previous findings [41,42]. However, comparing the two methods revealed that M – H samples exhibited a slight decrease in nitrogen content (from 0.23 % to 0.19 %), compared to SH-Conv. This suggests that nitrogenous compounds degrade and volatilise more easily under microwave-assisted conditions. This may be due to the more efficient heating and molecular agitation provided by microwave irradiation. Sulfur content remained low across all samples, regardless of the hydrothermal carbonization method used. However, at 250 °C, both M – H and SH-Conv methods produced hydrochar with the lowest sulfur content (0.13 %), suggesting that elevated temperatures promote sulfur reduction. The low overall sulfur content across treatments supports the suitability of these hydrochars for soil applications as it minimizes the risk of phytotoxicity.

Biomass with low moisture and ash content and a high fixed carbon and volatile matter content is generally considered suitable for hydrochar production. Luo et al. (2023) [43], for instance, emphasized that biochar stability in soil is influenced by its chemical composition, including moisture content, which affects its suitability for carbon

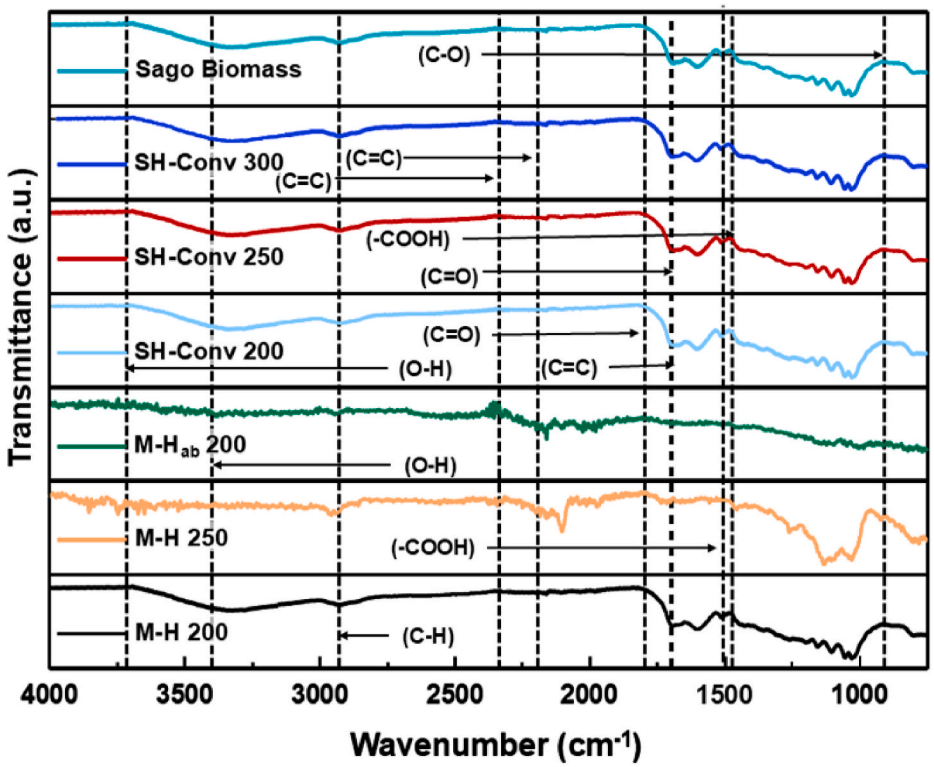


**Fig. 2.** The FT-IR spectrum of the sago biomass and hydrochars obtained with Microwave-Hydrochar (M – H) 200 °C, 250 °C, and Microwave-Hydrochar treated with 68.40 % sulfuric acid (Activated Microwave-Hydrochar) 200 °C; conventional heating (SH-Conv) 200 °C, 250 °C, and 300 °C.

sequestration applications. The initial sago biomass had a moisture content of 10.74 %, which was below the optimal threshold of 11 % for hydrothermal processing and aligned with values reported for similar feedstocks. Ghadge et al. (2022 noted that feedstocks with a moisture content below 11 % are ideal for hydrothermal liquefaction process, as they minimize water usage and enhance process efficiency) [44].

### 3.2. Hydrochar FTIR characterization

Fig. 2 shows that Fourier-transform infrared (FTIR) was used to analyze the chemical changes in sago-derived hydrochars produced by microwave and conventional hydrothermal carbonization at different temperatures.

Overall, the spectral characteristics collectively revealed that the hydrothermal treatment significantly altered the surface chemistry of the samples. The raw biomass exhibited major absorption bands, including broad peaks indicative of O-H group vibrations due to hydroxyl functionalities and moisture, and a distinct absorption band at about 912 $cm^{-1}$ representing C-H stretching. The observed peaks gradually diminished or disappeared in the hydrochar samples, especially at higher temperatures, indicating a loss of hydroxyl groups due to dehydration and condensation processes.

The region between 1250 and 1800 $cm^{-1}$, which contains characteristic peaks for alkanes, aromatics, and polyphenols (the aromatic ring contains O-H, C=C, and C=O functional groups), showed a decrease in intensity as the temperature of the hydrochar produced by microwave-assisted hydrothermal processing increased. A prominent peak at 1475-1693 $cm^{-1}$, indicative of polyphenolic structures, decreased moderately, suggesting partial degradation of these compounds. Peaks related to phenols, ethers, esters, and alcohols (the process includes O-H bending and C-O stretching motions) also decreased, reflecting the breakdown of oxygenated functional groups during carbonization.

These changes suggest a gradual decrease in surface polarity and acidic functional groups as the hydrothermal temperature increases. While this trend was generally more pronounced in SH-Conv hydrochars, the peaks related to O-H bonds between 2929 $cm^{-1}$ and 3716 $cm^{-1}$ were still clearly present, indicating that dehydration was not complete. The partial retention of these groups suggests the presence of residual hydroxyl functionalities, possibly due to incomplete decomposition of cellulose or hemicellulose-derived structures. In contrast, the M − H hydrochar exhibited these peaks at slightly lower intensities, implying a different or more selective transformation pathway under microwave-assisted heating. These observations are consistent with recent findings on the microwave-assisted hydrothermal processing of sago biomass [45,46].

Previous studies have reported a significant reduction or near-complete elimination of surface functional groups, including O-H, C=O, and C-O, at hydrothermal processing temperatures of around 400 °C due to extensive thermal degradation and dehydration reactions. In contrast, our study focuses on a lower temperature range of 200–300 °C, where these transformations are less complete but still observable. Within this moderate temperature range, we observed a progressive attenuation of functional group peaks, such as those corresponding to hydroxyl and carbonyl groups. This indicates ongoing deoxygenation and condensation reactions [47]. This suggests that, although complete removal of polar functionalities may require processing temperatures of at least 400 °C, significant structural evolution occurs at temperatures between 200 and 300 °C [48]. These findings provide valuable insight into intermediate chemical transitions during hydrothermal treatment and highlight the potential to tailor hydrochar properties without resorting to extreme thermal conditions.

In addition to the unactivated samples, the FTIR spectrum of the activated microwave-hydrochar (M-$H_{ab}$) showed evidence of further structural modifications. Notably, the intensity of the broad O-H stretching band around 3400 $cm^{-1}$ decreased significantly, indicating a reduction in surface hydroxyl groups due to enhanced dehydration and condensation during activation. Similarly, the intensity of the C=O stretching vibrations at around 1700 $cm^{-1}$ and the C-O stretching bands in the 1000-1300 $cm^{-1}$ range diminished, suggesting the removal of oxygenated functional groups, such as carboxylic acids, esters, and alcohols. These spectral changes reflect a higher degree of carbonization and aromatic character in the activated material. Compared to the unactivated M − H sample, the activated version exhibits greater structural stability and a more hydrophobic surface chemistry, which are advantageous for applications such as adsorption and energy storage. These findings further confirm that the activation step significantly enhances the chemical and functional properties of microwave-derived hydrochar.

### 3.3. Surface area and porosity determination

BET surface area and pore structure investigations of hydrochars prepared from sago biomass by microwave-assisted hydrothermal carbonization (M − H) and conventional heating (SH-Conv), with and without sulfuric acid activation, are presented in Table 2. The data illustrate the significant differences in structural and physicochemical properties resulting from the thermal treatment methods and acid activation. Specifically, at a hydrothermal carbonization temperature of 200 °C, the specific surface area of hydrochar produced by the microwave-assisted hydrothermal (M − H) method increased from 10.05 $m^2/g$ for a non-activated sample to 179.8 $m^2/g$ after acid-activation, as determined by BET analysis. After acid activation, the surface area of the SH-Conv hydrochar ranges from 4.01 m2/g to 57.9 m2/g, indicating that treatment and acid activation both significantly enhance surface area and porosity.

The low surface areas observed in non-activated hydrochar can be attributed to dense and poorly developed structures formed during the hydrothermal carbonization process. In non-activated samples, organic volatiles and tars produced during carbonization can condense and redeposit in internal pore spaces, blocking pores and reducing surface accessibility. This phenomenon is particularly pronounced in hydrochars produced by conventional heating, as slower heating rates and uneven thermal gradients facilitate tar condensation and limit effective volatile release [38,49].

Significant increases in both the total volume and surface area of M − H hydrochar were observed following acid activation, while a substantial increase in surface area was primarily observed in SH-Conv hydrochars. This increase is associated with several chemical and structural modifications initiated by sulfuric acid: (1) pore activation: $H_2SO_4$ acts as a dehydrating agent, aiding in the removal of water and other volatile species occupying pore spaces, thereby promoting pore development and increasing structural openness; (2) surface etching and oxidation: acid treatment introduces $SO_3H$ groups and oxidizes carbonaceous materials, resulting in the degradation of residual tars and the enlargement of existing pores by chemical etching, threby improving accessibility to internal surfaces and freeing previously blocked miro- and mesopores [50].

Furthermore, when comparing M − H hydrochars to those produced via SH-Conv, the former showed a greater degree of structural development and more favourable pore distribution following acid activation. This improvement is likely due to the distinct volumetric heating mechanism of microwaves, which creates localised high-pressure environments that disrupt biomass matrices more efficiently than conventional conductive heating [51].

The hydrochars synthesized using microwave-assisted hydrothermal treatment at 250 °C showed significantly enhanced structural and surface characteristics, demonstrating the impact of this process at elevated temperatures.

These improvements in porosity and surface area are critical to the functional performance of hydrochar, particularly in applications such as adsorption, catalysis, and soil amendment. The effectiveness of microwave-assisted hydrothermal carbonization combined with acid

**Table 2**
BET surface area and pore characteristics of the sago biomass and the hydrochars obtained at 200, 250, and 300 °C.

| Hydrochar samples | pH | Bulk density ($m^3$/g) | BET surface area ($m^2$/g) | Total pore volume ($cm^3$/g) | Mean pore diameter (nm) |
|---|---|---|---|---|---|
| Sago Biomass | 4.5 ± 0.23 | 0.36 ± 0.11 | 4.24 ± 0.14 | 0.02 ± 0.12 | 1.12 ± 0.18 |
| M − H 200 | 7.8 ± 0.14 | 0.74 ± 0.19 | 10.05 ± 0.05 | 0.12 ± 0.11 | 1.64 ± 0.16 |
| M − H 250 | 9.60 ± 0.09 | 0.91 ± 0.13 | 20.24 ± 0.14 | 0.02 ± 0.01 | 1.22 ± 0.10 |
| SH-Conv 200 | 7.25 ± 0.17 | 0.03 ± 0.17 | 4.01 ± 0.20 | 0.03 ± 0.05 | 1.10 ± 0.15 |
| SH-Conv 250 | 9.50 ± 0.12 | 0.05 ± 0.17 | 7.03 ± 0.13 | 0.03 ± 0.05 | 1.40 ± 0.18 |
| SH-Conv 300 | 10.06 ± 0.02 | 0.09 ± 0.15 | 57.9 ± 0.17 | 0.14 ± 0.13 | 1.22 ± 0.12 |
| M-$H_{ab}$ 200 | 6.65 ± 0.28 | 1.38 ± 0.28 | 179.8 ± 0.25 | 0.48 ± 0.12 | 1.68 ± 0.16 |

M-H: Microwave hydrochar; SH-Conv: Sago hydrochar – Conventional heating; M-$H_{ab}$: Activated Microwave-hydrochar.

activation suggests a viable strategy for tailoring hydrochar properties for specific end-uses.

### 3.4. Bulk density

Both the hydrothermal temperature and the heating method used influenced the bulk density. The raw sago biomass had a bulk density of 0.36 $m^3$/g. Following hydrothermal treatment, the bulk density of the hydrochars produced using the microwave-assisted method increased with temperature, rising from 0.74 $m^3$/g at 200 °C to 0.91 $m^3$/g at 250 °C. By contrast, the bulk density of hydrochars produced by the conventional (SH-Conv) method increased from 0.03 $m^3$/g at 200 °C to 0.09 $m^3$/g at 300 °C. The acid-activated M − H hydrochar (M-$H_{ab}$) exhibited the highest bulk density, at 1.38 $m^3$/g. These trends suggest that the heating method and activation significantly affect the structural compaction and densification of the resulting hydrochars [52–54].

### 3.5. pH of sago biomass and hydrochar

As shown in Table 2, the pH of raw sago biomass is approximately 4.5. Following hydrothermal carbonization, the pH of the resulting hydrochars increased significantly due to the degradation of acidic functional groups and the concentration of alkaline minerals, such as potassium, calcium, and magnesium, in the solid phase [55,56]. The pH values of hydrochars produced by microwave-assisted heating (M − H) ranged from 7.25 to 9.6, whereas those produced by conventional heating (SH-Conv) ranged from 7.25 to 10.06, indicating a shift towards alkalinity. In contrast, the acid-activated, microwave-derived hydrochar (M-$H_{ab}$) exhibited a slightly acidic pH of 6.65.

These decreases in pH after activation are attributed to the

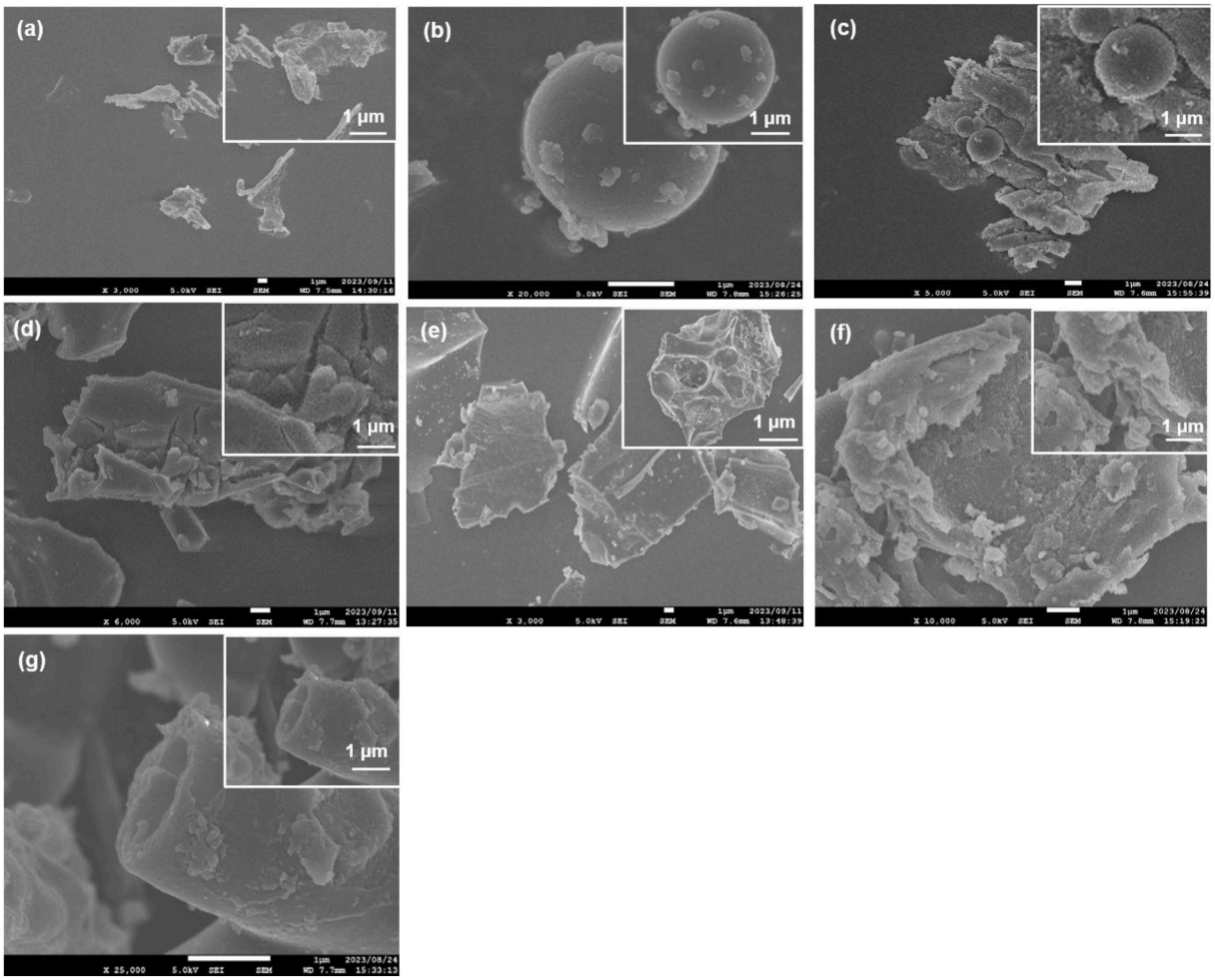


**Fig. 3.** Surface structure by SEM analysis (a), sago biomass at 3000 X, b-g obtained at 200, 250, and 300 °C for different hydrochars: (b), M − H 200 at 25,000 X (c), M − H 250 at 5000 X (d), SH-Conv 200 at 6000 X (e), SH-Conv 250 at 3000 X (f), SH-Conv 300 at 10,000 and M − H $200_{ab}$ at 25,000 X (g).

introduction of acidic functional groups (e.g., carboxylic, phenolic, and lactonic groups) onto the hydrochar surface during acid activation. The acid treatment removes some mineral ash components and introduces oxygen-containing functionalities, which increase surface acidity. These changes lower the overall pH of the hydrochar despite its prior alkalinity. This observation is consistent with previous studies reporting a pH decline following acid activation due to enhanced surface oxygenation and reduced mineral content [57,58]. Understanding these changes is crucial for tailoring hydrochar for specific applications, such as adsorption or catalysis, where surface acidity plays a key role.

### 3.6. Morphology and structural characteristics

SEM analysis (Fig. 3a–g) shows the shape and particle size distribution (PSD) of sago biomass and hydrochars produced at different hydrothermal temperatures. The raw biomass had almost no visible pores and exhibited a dense, fibrous morphology with a fragmented structure, with most particles measuring less than 2 μm in size [59]. At 200 °C (see Fig. 3b & g), SEM images revealed a well-developed carbon sphere morphology, with an average particle size below 1.0 μm. This indicates the presence of residual carbonaceous fragments or inorganic matter. At 250 °C (Fig. 3c), the hydrochars had smaller spiral pores and well-defined openings, most likely related to the emission of volatile chemicals and thermal decomposition that created these channel-like structures. However, the hydrochars produced at 300 °C (see Fig. 3f) had a more fragmented and disordered surface morphology, which is consistent with the findings of previous studies [60].

The observed changes in surface area and morphology after sulfonation are related to several mechanisms. Firstly, sulfuric acid acts as a dehydrating agent, removing volatile components and opening up the pore structure. In addition, acid treatment can introduce sulfonic acid groups (-$SO_3H$) to the surface, which can further increase porosity by breaking down carbonaceous material and promoting the formation of new pores. This chemical modification results in a more developed structure, which is beneficial for applications that require a large surface area, such as catalysis and adsorption.

In our study, hydrothermal carbonization experiments were conducted at temperatures ranging from 200 °C to 300 °C. While we did not investigate hydrothermal behavior at temperatures above 300 °C, we refer to previous studies for comparative insights. For example, it has been reported that, as the reaction temperature increases from 260 °C to 340 °C, hydrochar particles tend to aggregate and cross-link into structures as large as 7.0 μm, likely due to nucleation and cellulose degradation at high temperature [61]. However, further increases in temperature, particularly under supercritical conditions, may cause these larger particles to break apart, resulting in smaller fragments and a broader particle size distribution [62]. Consequently, the particle size distribution at 340 °C resembled that of M – H 200, with around 70 % of particles measuring under 1.0 μm in diameter. It is important to note that these observations are based on prior work.

### 3.7. Crystallographic analysis and structural characteristics

X-ray diffraction (XRD) analysis was performed to investigate the crystalline structure of the hydrochars, as this can influence their physicochemical properties and potential applications. As shown in

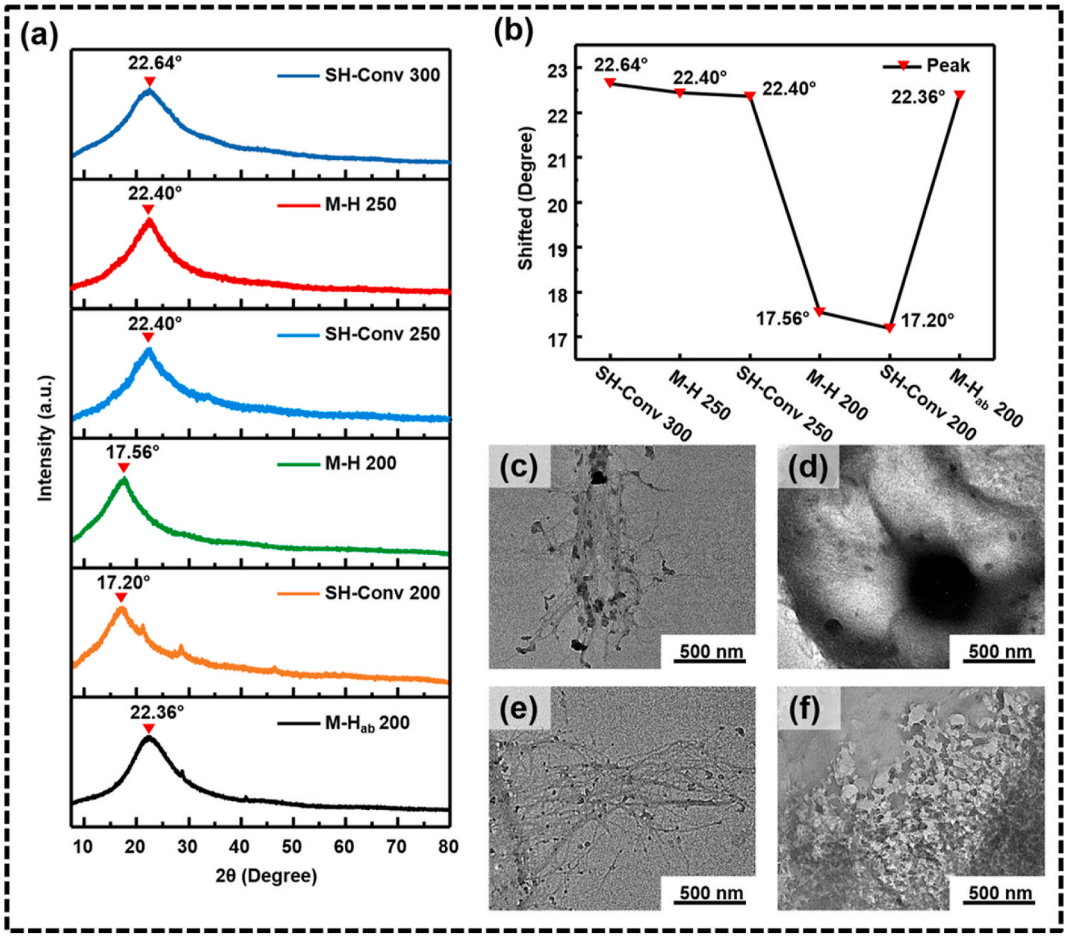


**Fig. 4.** (a), X-ray diffraction spectra (b), degree of peaks shift and transmission electron microscope images of sago biomass and hydrochars obtained at 200, 250, and 300 °C (c), Sago biomass (d), M – H 200 (e), M – H 250 and M – H $200_{ab}$ (f).

Fig. 4a, the XRD patterns of sago biomass and hydrochars produced via microwave-assisted (M − H) or conventional hydrothermal (SH-Conv) processing at various temperatures exhibit broad peaks centered at approximately 22.64°, 22.36°, and 22.40°. These peaks correspond to the (002) crystallographic plane, which is typically associated with turbostratic or graphitic carbon structures [63]. The presence of these (002) reflections suggests partial graphitization and structural ordering of the carbon matrix. The sharper, more intense peaks observed in the hydrochars compared with the raw biomass suggest an increase in structural regularity and crystallinity, likely resulting from the removal of amorphous components and thermal reorganization of carbon atoms during the hydrothermal process. Furthermore, the intensity and sharpness of the (002) peak are affected by temperature and duration of the treatment, reflecting changes in interlayer spacing and carbon domain size, as demonstrated in previous studies [64].

A noticeable shift in XRD peak positions was observed at 200 °C, particularly from approximately 17.56°–17.20° (see Fig. 4b). This shift suggests a change in the crystalline structure or phase composition of the material, likely due to the lower processing temperature. At these temperatures, the hydrochar is expected to retain partially ordered, cellulose-like crystalline structures such as cellulose I or II, which progressively degrade with increasing temperature [65]. These semi-crystalline structures tend to become increasingly disordered due to hydrothermal degradation, leading to the formation of more amorphous carbonaceous phases [66].

By contrast, at higher temperatures (≥280 °C), increased carbonization and the rearrangement of carbon atoms led to the formation of turbostratic or weakly graphitic domains, as evidenced by the emergence or intensification of the (002) peak at around 22°–23° [67]. The shift observed at lower temperatures is likely due to changes in crystallization kinetics that influence crystal size, lattice strain, and the balance between crystalline and amorphous domains. This transformation is consistent with the results of previous studies on the temperature-dependent structural evolution of biomass-derived hydrochars [68].

In general, lower temperatures may not provide sufficient energy for the formation of crystalline carbon, resulting in more disordered structures. However, at higher temperatures, more volatile organic compounds are released, contributing to the formation of more defined crystalline structures due to increased carbonization [69]. Interestingly, no direct relationship was found between crystallinity and fixed carbon content, suggesting that the orientation of the carbon structure may have a greater influence on crystallinity than its absolute concentration.

Further confirmation of the morphological characteristics observed is provided by TEM images (Fig. 4c–f) of the hydrochars at different magnifications. Both the SH-Conv and M − H treated hydrochars exhibit porous structures and significantly smaller particle sizes than the raw biomass. In particular, the particles in the M − H treated hydrochar predominantly range from 400 to 600 nm in size, with an average of around 500 nm (see Fig. 4d). These findings are consistent with previous studies on hydrochar and biochar materials, which reported similar nanoscale particle dimensions [70]. The reduction in particle size is likely due to the thermal degradation of biomass components and structural reorganization during the hydrothermal and microwave-assisted treatments.

TEM images of hydrochars carbonized at 200 °C for 1 h show structures resembling cellulose fibres, indicating limited biomass decomposition at this temperature. Increasing the residence time at 200 °C results in a more compact hydrochar morphology with smoother surfaces and better-defined pore structures. This transformation is attributed to the progressive breakdown of hemicellulose and the partial degradation of cellulose, which leads to structural rearrangement and increased porosity [71]. At higher treatment temperatures (e.g. 280–300 °C), the hydrochars exhibit a more fragmented and disordered morphology with smaller, more irregularly shaped particles, which is consistent with increased carbonization and thermal decomposition. Acid activation further enhances porosity and surface roughness by etching away volatile components and opening the pore network.

## 4. Potential application of hydrochar as a catalyst

The study demonstrates the remarkable potential of converting sago plant agricultural waste into carbon materials, specifically hydrochar, through microwave irradiation under controlled conditions. Initial results show that acidic hydrochar derived from microwave-assisted hydrothermal carbonization (M-$H_{ab}$) of sago is a highly effective catalyst for GTBE synthesis, achieving 99 % glycerol conversion and 59.9 % selectivity. These catalytic performances are attributed to its enhanced surface area, acidic functional groups, and porous structure.

This confirms previous research and highlights the significant yet untapped potential of sago biomass for renewable energy applications, as reported by Rambli et al. [21]. The use of hydrochar as a catalyst offers exciting opportunities for further exploration in this important area. This result highlights the outstanding catalytic capabilities of the hydrochar produced by MWHTC and confirms its potential to produce valuable products such as GTBE from renewable biomass sources. In contrast, other thermochemical methods, such as pyrolysis, typically produce less desirable results, while incineration produces mainly heat and $CO_2$, with limited applications in catalysis.

### 4.1. Catalyst characterization

The highly cross-linked macroporous structure and large average pore size of the sago hydrochar (M − H 200) increase its reactive properties, making it suitable for use as a catalyst. These increased pore sizes facilitate the conversion process by allowing relatively large molecules, such as glycerol, to reach the inner surface of the catalyst, as stated by Klepacova et al. (2007). Optimum catalytic performance was achieved using sago hydrochar (M-$H_{ab}$) under the following conditions: a temperature of 110 °C, a catalyst loading of 0.2 g; a reaction time of 1 h; and a TBA/Gly molar ratio of 6:1. Under these conditions, maximum glycerol conversion of 99 % was obtained, along with a selectivity of 59.9 % towards GTBE.

It exhibits significant surface and pore volume properties. According to Table 2, acid-activated, microwave-derived hydrochar (M-$H_{ab}$) exhibited a high surface area of 179.80 $m^2$/g and a pore volume of 0.48 $cm^3$/g. This indicates significant textural development after sulfuric acid treatment. These properties suggest that M-$H_{ab}$ has promising characteristics for catalytic applications, particularly due to its enhanced porosity and surface accessibility. MTBGs, DTBGs, and TTBGs were consistently present in the reaction products irrespective of the heating technique used. Interestingly, no glycerol-related side reactions were observed under these conditions.

### 4.2. Glycerol etherification aided by a microwave

During the MWHTC process, sago biomass undergoes a series of thermochemical reactions, primarily hydrolysis, dehydration, decarboxylation, and polymerization, under subcritical water conditions. The main components of the biomass (cellulose, hemicellulose, and lignin) are broken down into monomeric sugars and oligomers, which then convert into reactive intermediates such as furfurals, 5-hydroxymethylfurfural (HMF), and organic acids. These intermediates then undergo condensation, re-polymerization, and aromatization to form a carbon-rich hydrochar matrix. Microwave irradiation enhances these reactions by promoting rapid and uniform volumetric heating, thereby improving reaction kinetics and the selective formation of surface functionalities. The resulting hydrochar is enriched with oxygen-containing groups (e.g., –COOH, –OH, –C=O), which improve hydrophilicity and surface acidity, and contribute directly to catalytic properties in subsequent applications.

The glycerol etherification reaction catalyzed by acid-activated

microwave hydrochar (M-$H_{ab}$) demonstrated excellent performance, achieving 99 % glycerol conversion and 59.9 % selectivity towards high-value ethers. Product distribution analysis revealed that mono-*tert*-butyl glycerol ethers (MTBGs) constituted approximately 29.3 % of the product, di-*tert*-butyl glycerol ethers (DTBGs) constituted 10.8 %, and tri-*tert*-butyl glycerol ethers (TTBGs) constituted only 3.2 %. These findings are consistent with those from previous studies [72].

The low yield of TTBG can be attributed to steric hindrance caused by the bulky *tert*-butyl groups, which restrict further substitution following the formation of MTBG and DTBG. Furthermore, TTBG formation is less favourable without efficient water removal, since water shifts the reaction equilibrium backwards. Although TTBG was only detected in trace amounts in this study, previous research has shown that using water-removal techniques such as water-permselective membranes or adding zeolites can significantly increase the yield of higher glycerol ethers, such DTBG and TTBG [73,74].

The performance of the M-$H_{ab}$ catalyst is strongly influenced by its surface acidity rather than just its textural properties. As shown in Table 2, M-$H_{ab}$ exhibited a high surface area (179.80 $m^2/g$) and sufficient mesoporous pore volume (0.48 $cm^3/g$) with mesopores >10 nm, as well as enhanced acid site density due to sulfuric acid activation. These properties allow for the effective diffusion and adsorption of reactant molecules, facilitating the protonation of *tert*-butyl alcohol (TBA) and the subsequent formation of glycerol ethers. These results highlight the potential of sago-derived M-$H_{ab}$ as a sustainable, low-cost catalyst for glycerol etherification reactions.

### 4.3. Comparison of sago hydrochar (M – H 200) with other reported catalysts

The study examined the etherification of glycerol with *tert*-butyl alcohol (TBA) using different catalysts. Sago hydrochar (M – H 200) demonstrated the best catalytic performance, achieving 99 % glycerol conversion and 59.9 % GTBE selectivity in only 1 h at 110 °C. This result is comparable to that of Amberlyst 15, a widely used commercial resin which, under similar conditions, produced slightly lower selectivity as reported in previous studies [75]. By contrast, catalysts such as C(10) AlPO(1.5)-250 and p-styrene sulfonic acid produced significantly lower glycerol conversion rates (78–85 %) under similar or slightly harsher conditions (120 °C for 2–4 h), highlighting the M – H 200 catalyst's efficiency in facilitating etherification reactions (see Table 3).

The MWHTC method is a more sustainable alternative to traditional processes such as pyrolysis and incineration, primarily due to its ability to operate at lower temperatures and pressures. The results of this process are a reduced high-carbon hydrochar (53.55 %), which has been identified as a promising material for eco-friendly applications, including carbon capture and renewable energy generation [76].

Notwithstanding the encouraging outcomes observed with sago hydrochar, the catalysts that are typically in the extant literature operate at elevated reaction temperatures but require shorter reaction times. For instance, the utilisation of caesium-exchange tungstophosphoric acid, supported by tin oxide, yielded the highest documented GTBE yield (40 %). However, the catalyst utilised in the aforementioned study accounted for 27 wt% of the total glycerol, which is more than six times the amount of catalyst used in the present study. These findings serve to highlight the efficiency of sago hydrochar in terms of catalyst loading [77].

### 4.4. Reusability and stability of hydrochar as a catalyst

The reusability of the acid-activated sago hydrochar catalyst (M – H 200) was investigated over five consecutive etherification cycles, the results of which are presented in Fig. 5. The total GTBE yield remained relatively stable during the first three cycles, with respective yields of 56.9 %, 56.2 %, and 56.2 %. However, noticeable declines in catalytic performance occurred in the fourth and fifth cycles, with yields dropping to 48 % and 40 %, respectively.

The catalyst's stable performance in the first three cycles indicates good short-term reusability and structural resilience. The subsequent decrease in activity could be due to several factors, including the partial deactivation of active sites, the fouling of the surface by reaction by-products, or the slight structural degradation of the porous framework. Additionally, residual glycerol or *tert*-butyl ethers adsorbed on the surface may block access to catalytic sites over time [81]. These results suggest that, although M – H 200 shows promising reusability, its long-term application may require regeneration treatments or optimized reaction conditions to mitigate catalyst deactivation [82].

### 4.5. Prospective developments and their commercial viability

While the laboratory-scale results of MWHTC are promising, challenges related to reactor design, raw material availability, and cost-effectiveness must be addressed if this process is to be scaled up. A critical evaluation of the economic viability of hydrochar as a catalyst must be undertaken in conjunction with a comprehensive assessment of

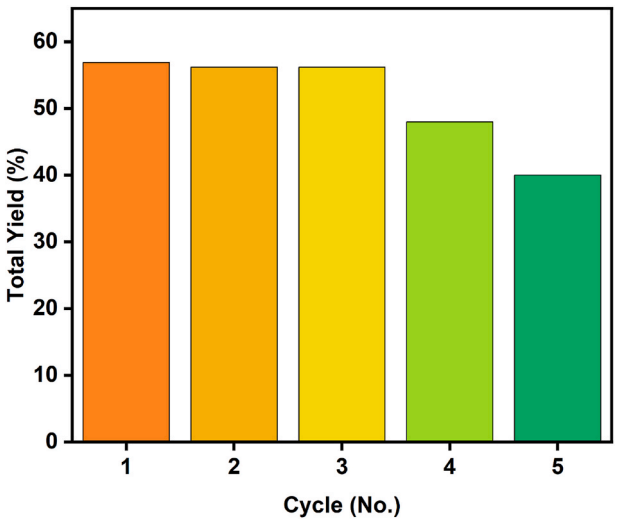


**Fig. 5.** GTBE yield from sago-based hydrochar catalyst remained stable over three cycles, with reduced performance in subsequent cycles (The GTBE yield remained stable over the first three cycles (56.9 %, 56.2 %, and 56.2 %), with a gradual decline in the fourth and fifth cycles (48 % and 40 %, respectively).

**Table 3**
Literature-based comparison of catalysts.

| Catalyst | Condition and Dosage | Conversion (%) | Time (h) | Selectivity (%) | | References |
|---|---|---|---|---|---|---|
| | | | | MTBG | GTBE | |
| Amberlyst 15 | 4:1 dose-7.5 wt% | 97 | 8 | 29.7 | 30.3 | [78] |
| *p*-styrene sulfonic acid | 4:1 dose-5 wt.% | 81 | 1.5 | 94.0 | 6.0 | [79] |
| C(10)AlPO(1.5)-250 | 4:1 dose-5 wt.% | 83 | 1 | 76 | 23 | [80] |
| M – H 200 | 6:1 dose-5 wt.% | 99 | 1 | 37.2 | 59.9 | **present study** |

Reaction details: 0.2 g catalyst, 10.86 mmol glycerol, and 86.88 mmol TBA performed at 110 °C for 1 h.

its environmental implications. It is recommended that subsequent research endeavours focus on the optimization of the process, encompassing the examination of reaction time, temperature, and catalyst loadings. This will ensure the process's commercial viability on a larger scale [83,84]. Furthermore, there is a necessity for additional studies to be conducted to enhance the hydrochar synthesis process. The objective of these studies should be to ensure the maintenance of stable catalytic activity and the reduction of catalyst degradation over time.

## 5. Conclusion

This study sheds light on the hydrothermal carbonization (HTC) of sago biomass for producing functional hydrochar, focusing particularly on its use as a catalyst in glycerol etherification. The results show that sago biomass is a promising, sustainable source of hydrochar with enhanced physicochemical and catalytic properties. Microwave-assisted hydrothermal carbonization (MWHTC) at 200 °C was found to be more effective than conventional heating, yielding a higher hydrochar output of 29.8 % with reduced volatile matter and improved fixed carbon content. The carbonization process also decreased the hydrogen and oxygen content, enhancing hydrophobicity and thermal stability. The resulting hydrochar exhibited an alkaline pH (6.65), indicative of reduced acidic functional groups and increased ash content, both of which are favourable for catalytic activity. Physicochemical analysis revealed that acid-activated microwave hydrochar (M-$H_{ab}$) had a BET surface area of 179.8 $m^2/g$ and a pore volume of 0.48 $cm^3/g$, with mesopores >10 nm enabling efficient diffusion of reactants to active sites. FTIR and XRD analyses confirmed the removal of polar functional groups and the enrichment of inorganic content with increasing treatment temperature. Under optimized reaction conditions (110 °C for 1 h with 0.2 g of catalyst and a TBA/Gly molar ratio of 6:1), the M-$H_{ab}$ catalyst demonstrated excellent performance, achieving 99 % glycerol conversion and 59.9 % selectivity toward GTBE. The catalyst also exhibited good short-term reusability. The GTBE yield remained stable over the first three cycles (56.9 %, 56.2 %, and 56.2 %), before gradually declining in the fourth and fifth cycles (48 % and 40 %, respectively). This is likely due to fouling or deactivation of active sites. These results suggest that sago-derived hydrochar has potential as an environmentally friendly, low-cost catalyst. Overall, MWHTC is validated as a viable and efficient method for producing hydrochar from sago biomass. However, future work should explore catalyst regeneration and long-term performance under continuous operation to further assess its industrial potential.

## CRediT authorship contribution statement

**Jakaria Rambli:** Writing – original draft, Visualization, Validation, Methodology, Investigation, Formal analysis, Data curation, Conceptualization. **Armando T. Quitain:** Writing – review & editing, Visualization, Validation, Supervision, Project administration, Methodology, Investigation, Funding acquisition, Conceptualization. **Ramin Khezri:** Writing – review & editing, Investigation. **Wan Azlina Wan Ab Karim Ghani:** Writing – review & editing, Formal analysis. **Suttichai Assabumrungrat:** Writing – review & editing, Funding acquisition. **Tetsuya Kida:** Validation, Supervision, Resources, Methodology, Investigation, Formal analysis, Conceptualization.

## Conflict of interest

The authors would like to declare that there was no conflict of interest in this study.

## Acknowledgments

The authors would like to acknowledge Sarawak Premier Office for funding assistance for Jakaria Rambli's study and stay in Japan. This work was also partially supported by JSPS-NRCT Bilateral Joint Research Project (JPJSBP120239202 (JSPS), N10A660366 (NRCT)). The support and assistance of all personnel, colleagues and research assistants in performing experiments, and in completing this paper are highly acknowledged.

## Nomenclature

| | |
|---|---|
| $\theta$ | X-ray diffraction angle (°) |
| *μL* | microliter |
| *ar* | atomic ratio |
| *C* | Carbon |
| $CO_2$ | Carbon dioxide |
| *FC* | fixed carbon |
| *GHz* | gigahertz |
| *g* | gram |
| *H* | Hydrogen |
| *h* | hour |
| *K* | *kelvin* |
| *kg* | kilogram |
| *mm* | millimeter |
| *mJ* | millijoule |
| *mL* | milliliter |
| *N* | Nitrogen |
| *O* | Oxygen |
| *rpm* | *revolutions per minute* |
| *SB* | sago bark |
| $S_i$ | product selectivity ($S_i$) |
| *S* | Sulfur |
| *Tg* | Teragram |
| *VM* | volatile matter |
| *W* | watt |
| *wt.%* | weight percent |
| $X_{Gly}$ | conversion of glycerol |
| *Y* | yield |

### *Abbreviation*

| | |
|---|---|
| BET | *Brunauer-Emmet-Teller* |
| DTBGs | di-*tert*-butyl ether |
| DTBG 1 | di-*tert*-butyl ether of glycerol 1 |
| DTBG 2 | di-*tert*-butyl ether of glycerol 2 |
| DTG | differential thermogravimetry |
| FT-IR | Fourier Transform Infrared Spectrometer |
| GC-MS | gas chromatography-mass spectrometry |
| GTBE | glycerol *tert*-butyl ether |
| Gly | Glycerol |
| HHV | higher heating value |
| HTC | hydrothermal carbonization |
| h-GTBE | high ethers |
| IB | isobutylene |
| LCAs | Life cycle assessments |
| M-$H_{ab}$ | Activated microwave-hydrochar |
| M-H | Microwave Hydrochar |
| MWHTC | Microwave hydrothermal carbonization |
| MTBGs | mono-*tert*-butyl ether |
| MTBG 1 | mono-*tert*-butyl ether of glycerol 1 |
| MTBG 2 | mono-*tert*-butyl ether of glycerol 2 |
| PSD | particle size distribution |
| SEM | Scanning Electron Microscopy |
| SH | Sago Hydrochar |
| SH-Conv | Sago Hydrochar-Conventional heating |
| TBA | *tert*-butyl alcohol |
| TEM | Transmission Electron Microscope |
| TGA | thermogravimetric analysis |
| TTBGs | tri-*tert*-butyl ether of glycerol |
| XRD | X-ray diffraction |

## Data availability

Data will be made available on request.

## References


[1] J. Rambli, W.A. Wan Abd Karim Ghani, M.A. Mohd Salleh, Characterization of sago-based biochar as potential feedstock for solid fuel, J. Energy Saf. Technol. (JEST) 1 (2018), https://doi.org/10.11113/jest.v1n2.16.

[2] N. Jain, A. Bhatia, H. Pathak, Emission of air pollutants from crop residue burning in India, Aerosol Air Qual. Res. 14 (2014) 422–430, https://doi.org/10.4209/aaqr.2013.01.0031.

[3] S. Bhuvaneshwari, H. Hettiarachchi, J.N. Meegoda, Crop residue burning in India: policy challenges and potential solutions, Int. J. Environ. Res. Publ. Health 16 (2019), https://doi.org/10.3390/ijerph16050832.

[4] S.K. Lohan, H.S. Jat, A.K. Yadav, H.S. Sidhu, M.L. Jat, M. Choudhary, J.K. Peter, P. C. Sharma, Burning issues of paddy residue management in north-west states of India, Renew. Sustain. Energy Rev. 81 (2018) 693–706, https://doi.org/10.1016/j.rser.2017.08.057.

[5] R. Yevich, J.A. Logan, An assessment of biofuel use and burning of agricultural waste in the developing world, Glob. Biogeochem. Cycles 17 (2003), https://doi.org/10.1029/2002gb001952.

[6] P.K. Gupta, S. Sahai, N. Singh, C.K. Dixit, D.P. Singh, C. Sharma, M.K. Tiwari, R. K. Gupta, S.C. Garg, Residue burning in rice-wheat cropping system: causes and implications, Curr. Sci. 87 (2004) 1713–1717.

[7] B. Zhao, D. O'Connor, J. Zhang, T. Peng, Z. Shen, D.C.W. Tsang, D. Hou, Effect of pyrolysis temperature, heating rate, and residence time on rapeseed stem derived biochar, J. Clean. Prod. 174 (2018) 977–987, https://doi.org/10.1016/j.jclepro.2017.11.013.

[8] S. Ge, P.N.Y. Yek, Y.W. Cheng, C. Xia, W.A. Wan Mahari, R.K. Liew, W. Peng, T. Q. Yuan, M. Tabatabaei, M. Aghbashlo, C. Sonne, S.S. Lam, Progress in microwave pyrolysis conversion of agricultural waste to value-added biofuels: a batch to continuous approach, Renew. Sustain. Energy Rev. 135 (2021), https://doi.org/10.1016/j.rser.2020.110148.

[9] N. Hossain, S. Nizamuddin, G. Griffin, P. Selvakannan, N.M. Mubarak, T.M. I. Mahlia, Synthesis and characterization of rice husk biochar via hydrothermal carbonization for wastewater treatment and biofuel production, Sci. Rep. 10 (2020), https://doi.org/10.1038/s41598-020-75936-3.

[10] M.T. Ravanchi, S. Sahebdelfar, Catalytic conversions of CO 2 to help mitigate climate change : recent process developments, Process Saf. Environ. Prot. 145 (2021) 172–194, https://doi.org/10.1016/j.psep.2020.08.003.

[11] G. Skouteris, D. Saroj, P. Melidis, F.I. Hai, S. Ouki, The effect of activated carbon addition on membrane bioreactor processes for wastewater treatment and reclamation - a critical review, Bioresour. Technol. 185 (2015) 399–410, https://doi.org/10.1016/j.biortech.2015.03.010.

[12] S. Ghysels, F. Ronsse, D. Dickinson, W. Prins, Production and characterization of slow pyrolysis biochar from lignin-rich digested stillage from lignocellulosic ethanol production, Biomass Bioenergy 122 (2019) 349–360, https://doi.org/10.1016/j.biombioe.2019.01.040.

[13] X. Ge, Y. Cao, B. Zhou, X. Wang, Z. Yang, M.H. Li, Biochar addition increases subsurface soil microbial biomass but has limited effects on soil CO2 emissions in subtropical moso bamboo plantations, Appl. Soil Ecol. 142 (2019) 155–165, https://doi.org/10.1016/j.apsoil.2019.04.021.

[14] M.K. Awasthi, Y. Duan, S.K. Awasthi, T. Liu, Z. Zhang, Influence of bamboo biochar on mitigating greenhouse gas emissions and nitrogen loss during poultry manure composting, Bioresour. Technol. 303 (2020), https://doi.org/10.1016/j.biortech.2020.122952.

[15] Y. Liu, X. Zhu, F. Qian, S. Zhang, J. Chen, Magnetic activated carbon prepared from rice straw-derived hydrochar for triclosan removal, RSC Adv. 4 (2014) 63620–63626, https://doi.org/10.1039/C4RA11815D.

[16] S. Wang, G. Dai, H. Yang, Z. Luo, Lignocellulosic biomass pyrolysis mechanism: a state-of-the-art review, Prog. Energy Combust. Sci. 62 (2017) 33–86, https://doi.org/10.1016/j.pecs.2017.05.004.

[17] J. Wu, D. Ren, X. Zhang, Z. Chen, S. Zhang, S. Li, L. Fu, The adsorption properties of biochar derived from woody plants or bamboo for cadmium in aqueous solution, Desalination Water Treat. 160 (2019) 268–275, https://doi.org/10.5004/dwt.2019.24174.

[18] 2019 J. Rambli, Evaluation of biochar from Sago (Metroxylon Spp.) as a potential solid, Fuel 14 (2019) 1928–1940.

[19] S.M.A. Mahanim, I. Wan Asma, J. Rafidah, E. Puad, H. Shaharuddin, Production of activated carbon from industrial bamboo wastes, J. Trop. For. Sci. 23 (2011) 417–424.

[20] T.H. Rasyid, Y. Kusumawaty, S. Hadi, The utilization of sago waste: prospect and challenges, in: IOP Conf Ser Earth Environ Sci, Institute of Physics Publishing, 2020, https://doi.org/10.1088/1755-1315/415/1/012023.

[21] J. Rambli, W.A. Wan Abd Karim Ghani, M.A. Mohd Salleh, Characterization of sago-based biochar as potential feedstock for solid fuel, J. Energy Saf. Technol. (JEST) 1 (2018), https://doi.org/10.11113/jest.v1n2.16.

[22] J. Rambli, W. Azlina, W. Ab, K. Ghani, M. Amran, M. Salleh, R. Khezri, Sago-Derived Biochar, 2019.

[23] Z. Liu, G. Han, Production of solid fuel biochar from waste biomass by low temperature pyrolysis, Fuel (2015), https://doi.org/10.1016/j.fuel.2015.05.032.

[24] S. Masoumi, V.B. Borugadda, S. Nanda, A.K. Dalai, 2021-Hydrochar A review on its production technologies.pdf, Catalysts 11 (2021) 939.

[25] Z. Xu, R. Dou, F. Gao, Y. Chen, L. Leng, S.M. Osman, R. Luque, Bio-adhesives derived from sewage sludge via hydrothermal carbonization : influence of aqueous phase recycling, Chem. Eng. J. 490 (2024) 151685, https://doi.org/10.1016/j.cej.2024.151685.

[26] D. Kim, K. Yoshikawa, K.Y. Park, Characteristics of biochar obtained by hydrothermal carbonization of cellulose for renewable energy, Energies (Basel) (2015), https://doi.org/10.3390/en81212412.

[27] ASTM D 7582-10, Standard test methods for proximate analysis of coal and coke by macro, Program i (2012) 1–9, https://doi.org/10.1520/D7582.

[28] D. Özçimen, An Approach to the Characterization of Biochar and Bio-Oil, Vildiz Technical University, Turkey, 2010, pp. 1–16.

[29] K. Klepáčová, D. Mravec, A. Kaszonyi, M. Bajus, Etherification of glycerol and ethylene glycol by isobutylene, Appl. Catal. Gen. 328 (2007) 1–13, https://doi.org/10.1016/j.apcata.2007.03.031.

[30] K. Klepáčová, D. Mravec, A. Kaszonyi, M. Bajus, Etherification of glycerol and ethylene glycol by isobutylene, Appl. Catal. Gen. 328 (2007) 1–13, https://doi.org/10.1016/j.apcata.2007.03.031.

[31] J.F. Izquierdo, P.R. Outón, M. Galán, L. Jutglar, M. Villarrubia, M.P. Hermo, X. Ariza, I. Fernández, Ethers of glycerol and isoamylenes as biodiesel additives: synthesis and characterization, Chem. Eng. Trans. 32 (2013) 877–882, https://doi.org/10.3303/CET1332147.

[32] Y.L. Kam, J.K.C.N. Agutaya, A.T. Quitain, Y. Ogasawara, M. Sasaki, M.K. Lam, S. Yusup, S. Assabumrungrat, T. Kida, In-situ transesterification of microalgae using carbon-based catalyst under pulsed microwave irradiation, Biomass Bioenergy 168 (2023) 106662, https://doi.org/10.1016/j.biombioe.2022.106662.

[33] J. Sun, F. He, Y. Pan, Z. Zhang, Effects of pyrolysis temperature and residence time on physicochemical properties of different biochar types, Acta Agric. Scand B Soil Plant Sci. 67 (2017) 12–22, https://doi.org/10.1080/09064710.2016.1214745.

[34] W. Yang, H. Wang, M. Zhang, J. Zhu, J. Zhou, S. Wu, Fuel properties and combustion kinetics of hydrochar prepared by hydrothermal carbonization of bamboo, Bioresour. Technol. 205 (2016) 199–204, https://doi.org/10.1016/j.biortech.2016.01.068.

[35] A. Palamanit, P. Khongphakdi, Y. Tirawanichakul, N. Phusunti, Investigation of yields and qualities of pyrolysis products obtained from oil palm biomass using an agitated bed pyrolysis reactor, Biofuel Res. J. 6 (2019) 1065–1079, https://doi.org/10.18331/BRJ2019.6.4.3.

[36] A. Ahmed, M.S. Abu Bakar, R. Hamdani, Y.K. Park, S.S. Lam, R.S. Sukri, M. Hussain, K. Majeed, N. Phusunti, F. Jamil, M. Aslam, Valorization of underutilized waste biomass from invasive species to produce biochar for energy and other value-added applications, Environ. Res. 186 (2020), https://doi.org/10.1016/j.envres.2020.109596.

[37] A. Tomczyk, Biochar physicochemical properties : pyrolysis temperature and feedstock kind effects, Rev. Environ. Sci. Biotechnol. 19 (2020) 191–215, https://doi.org/10.1007/s11157-020-09523-3.

[38] Y. Zhang, Q. Jiang, W. Xie, Y. Wang, J. Kang, Effects of temperature, time and acidity of hydrothermal carbonization on the hydrochar properties and nitrogen recovery from corn stover, Biomass Bioenergy 122 (2019) 175–182, https://doi.org/10.1016/j.biombioe.2019.01.035.

[39] S. Yu, J. Park, M. Kim, C. Ryu, J. Park, Characterization of biochar and byproducts from slow pyrolysis of hinoki cypress, Bioresour. Technol. Rep. 6 (2019) 217–222, https://doi.org/10.1016/j.biteb.2019.03.009.

[40] S. Roy, U. Kumar, P. Bhattacharyya, Synthesis and characterization of exfoliated biochar from four agricultural feedstock, Environ. Sci. Pollut. Control Ser. 26 (2019) 7272–7276, https://doi.org/10.1007/s11356-018-04117-7.

[41] R. Wahi, L.A. Chuah, Z. Ngaini, M.M. Nourouzi, T.S.Y. Choong, Esterification of M. sagu bark as an adsorbent for removal of emulsified oil, J. Environ. Chem. Eng. 2 (2014) 324–331, https://doi.org/10.1016/j.jece.2013.12.010.

[42] A.K. Sakhiya, A. Anand, P. Kaushal, Production, activation, and applications of biochar in recent times, Biochar 2 (2020) 253–285, https://doi.org/10.1007/s42773-020-00047-1.

[43] L. Luo, J. Wang, J. Lv, Z. Liu, T. Sun, Y. Yang, Y.G. Zhu, Carbon sequestration strategies in soil using biochar: advances, challenges, and opportunities, Environ. Sci. Technol. 57 (2023) 11357–11372, https://doi.org/10.1021/acs.est.3c02620.

[44] R. Ghadge, N. Nagwani, N. Saxena, S. Dasgupta, A. Sapre, Design and scale-up challenges in hydrothermal liquefaction process for biocrude production and its upgradation, Energy Convers. Manag. X 14 (2022), https://doi.org/10.1016/j.ecmx.2022.100223.

[45] T.H. Rasyid, Y. Kusumawaty, S. Hadi, The utilization of sago waste: prospect and challenges, in: IOP Conf Ser Earth Environ Sci, Institute of Physics Publishing, 2020, https://doi.org/10.1088/1755-1315/415/1/012023.

[46] S. Ramola, T. Mishra, G. Rana, R.K. Srivastava, Characterization and pollutant removal efficiency of biochar derived from baggase, bamboo and tyre, Environ. Monit. Assess. 186 (2014) 9023–9039, https://doi.org/10.1007/s10661-014-4062-5.

[47] M. Uchimiya, S.C. Chang, K.T. Klasson, Screening biochars for heavy metal retention in soil: role of oxygen functional groups, J. Hazard Mater. 190 (2011) 432–441, https://doi.org/10.1016/j.jhazmat.2011.03.063.

[48] M. Ahmad, A.U. Rajapaksha, J.E. Lim, M. Zhang, N. Bolan, D. Mohan, M. Vithanage, S.S. Lee, Y.S. Ok, Biochar as a sorbent for contaminant management in soil and water: a review, Chemosphere 99 (2014) 19–33, https://doi.org/10.1016/j.chemosphere.2013.10.071.

[49] I. Pavkov, M. Radojčin, Z. Stamenković, S. Bikić, M. Tomić, M. Bukurov, B. Despotović, Hydrothermal carbonization of agricultural biomass: characterization of hydrochar for energy production, Solid Fuel Chem. 56 (2022) 225–235, https://doi.org/10.3103/S0361521922030077.

[50] F. Meng, D. Wang, M. Zhang, Effects of different pretreatment methods on biochar properties from pyrolysis of corn stover, J. Energy Inst. 98 (2021) 294–302, https://doi.org/10.1016/j.joei.2021.07.008.
[51] A. Palamanit, P. Khongphakdi, Y. Tirawanichakul, N. Phusunti, Investigation of yields and qualities of pyrolysis products obtained from oil palm biomass using an agitated bed pyrolysis reactor, Biofuel Res. J. 6 (2019) 1065–1079, https://doi.org/10.18331/BRJ2019.6.4.3.
[52] C.E. Brewer, R.C.L.D. a Brown, Biochar Characterization and Engineering, Graduate Teses and Dissertations, 2012 12284 doi.org/12284.
[53] C.E. Brewer, V.J. Chuang, C.A. Masiello, H. Gonnermann, X. Gao, B. Dugan, L. E. Driver, P. Panzacchi, K. Zygourakis, C.A. Davies, New approaches to measuring biochar density and porosity, Biomass Bioenergy 66 (2014) 176–185, https://doi.org/10.1016/j.biombioe.2014.03.059.
[54] Z. Khanmohammadi, M. Afyuni, M.R. Mosaddeghi, Effect of pyrolysis temperature on chemical and physical properties of sewage sludge biochar, Waste Manag. Res. 33 (2015) 275–283, https://doi.org/10.1177/0734242X14565210.
[55] M.T. Reza, J.G. Lynam, M.H. Uddin, C.J. Coronella, Hydrothermal carbonization: fate of inorganics, Biomass Bioenergy 49 (2013) 86–94, https://doi.org/10.1016/j.biombioe.2012.12.004.
[56] J.A. Libra, K.S. Ro, C. Kammann, A. Funke, N.D. Berge, Y. Neubauer, M.M. Titirici, C. Fühner, O. Bens, J. Kern, K.H. Emmerich, Hydrothermal carbonization of biomass residuals: a comparative review of the chemistry, processes and applications of wet and dry pyrolysis, Biofuels 2 (2011) 71–106, https://doi.org/10.4155/bfs.10.81.
[57] L. Ye, J. Zhang, J. Zhao, Z. Luo, S. Tu, Y. Yin, Properties of biochar obtained from pyrolysis of bamboo shoot shell, J. Anal. Appl. Pyrolysis 114 (2015) 172–178, https://doi.org/10.1016/j.jaap.2015.05.016.
[58] M. Nasir, T. Rahmawati, F. Dara, Synthesis and characterization of biochar from crab shell by pyrolysis, in: IOP Conf Ser Mater Sci Eng, Institute of Physics Publishing, 2019, https://doi.org/10.1088/1757-899X/553/1/012031.
[59] C. Guizani, M. Jeguirim, S. Valin, L. Limousy, S. Salvador, Biomass chars: the effects of pyrolysis conditions on their morphology, structure, chemical properties and reactivity, Energies (Basel) 10 (2017), https://doi.org/10.3390/en10060796.
[60] B. Xiaofeng, Z. Xiaoqin, L. Zifu, N. Jiewen, B. Xue, Properties and applications of biochars derived from different biomass feedstock sources, Int. J. Agric. Biol. Eng. 10 (2017) 242–250, https://doi.org/10.3965/j.ijabe.20171002.2878.
[61] T. Wang, Y. Zhai, Y. Zhu, C. Li, G. Zeng, A review of the hydrothermal carbonization of biomass waste for hydrochar formation: process conditions, fundamentals, and physicochemical properties, Renew. Sustain. Energy Rev. 90 (2018) 223–247, https://doi.org/10.1016/j.rser.2018.03.071.
[62] G.A. Kahrilas, J. Blotevogel, E.R. Corrin, T. Borch, Downhole transformation of the hydraulic fracturing fluid biocide glutaraldehyde: implications for flowback and produced water quality, Environ. Sci. Technol. 50 (2016) 11414–11423, https://doi.org/10.1021/acs.est.6b02881.
[63] P. Ruz, S. Banerjee, M. Pandey, V. Sudarsan, P.U. Sastry, R.J. Kshirsagar, Structural evolution of turbostratic carbon: implications in H2 storage, Solid State Sci. 62 (2016) 105–111, https://doi.org/10.1016/j.solidstatesciences.2016.10.017.
[64] N. Saha, K. McGaughy, M.T. Reza, Elucidating hydrochar morphology and oxygen functionality change with hydrothermal treatment temperature ranging from subcritical to supercritical conditions, J. Anal. Appl. Pyrolysis 152 (2020) 104965, https://doi.org/10.1016/j.jaap.2020.104965.
[65] Y. Xie, F.Y. Li, X.J. Fan, S.J. Hu, X. Xiao, J.F. Wang, Components analysis of biochar based on near infrared spectroscopy technology, Chin. J. Anal. Chem. 46 (2018) 609–615, https://doi.org/10.1016/S1872-2040(17)61081-8.
[66] M. Mirkhalaf, R. Vadizadeh, Micro-mechanical modeling of semi-crystalline polymers: a review, Int. J. Solid Struct. 290 (2024), https://doi.org/10.1016/j.ijsolstr.2024.112691.
[67] D. Lachos-Perez, P. César Torres-Mayanga, E.R. Abaide, G.L. Zabot, F. De Castilhos, Hydrothermal carbonization and liquefaction: differences, progress, challenges, and opportunities, Bioresour. Technol. 343 (2022), https://doi.org/10.1016/j.biortech.2021.126084.
[68] R. Estevez, S. Lopez-Pedrajas, D. Luna, F.M. Bautista, Microwave-assisted etherification of glycerol with tert-butyl alcohol over amorphous organosilica-aluminum phosphates, Appl. Catal., B 213 (2017) 42–52, https://doi.org/10.1016/j.apcatb.2017.05.007.
[69] G.A. Kahrilas, J. Blotevogel, E.R. Corrin, T. Borch, Downhole transformation of the hydraulic fracturing fluid biocide glutaraldehyde: implications for flowback and produced water quality, Environ. Sci. Technol. 50 (2016) 11414–11423, https://doi.org/10.1021/acs.est.6b02881.
[70] W. Wang, A. Wang, Nanoscale clay minerals for functional ecomaterials: fabrication, applications, and future trends, in: Handbook of Ecomaterials, Springer International Publishing, 2018, pp. 1–82, https://doi.org/10.1007/978-3-319-48281-1_125-1.
[71] X. Zhu, Y. Liu, F. Qian, C. Zhou, S. Zhang, J. Chen, Preparation of magnetic porous carbon from waste hydrochar by simultaneous activation and magnetization for tetracycline removal, Bioresour. Technol. 154 (2014) 209–214, https://doi.org/10.1016/j.biortech.2013.12.019.
[72] R. Estevez, M.I. López, C. Jiménez-Sanchidrián, D. Luna, F.J. Romero-Salguero, F. M. Bautista, Etherification of glycerol with tert-butyl alcohol over sulfonated hybrid silicas, Appl. Catal. Gen. 526 (2016) 155–163, https://doi.org/10.1016/j.apcata.2016.08.019.
[73] F. Frusteri, F. Arena, G. Bonura, C. Cannilla, L. Spadaro, O. Di Blasi, Catalytic Etherification of Glycerol by tert-butyl Alcohol to Produce Oxygenated Additives for Diesel Fuel Applied Catalysis A : General Catalytic Etherification of Glycerol by Tert -butyl Alcohol to Produce Oxygenated Additives for Diesel Fuel, 2009, https://doi.org/10.1016/j.apcata.2009.07.037.
[74] C. Cannilla, G. Bonura, L. Frusteri, F. Frusteri, Glycerol etherification with TBA: high yield to poly-ethers using a membrane assisted batch reactor, Environ. Sci. Technol. 48 (2014) 6019–6026, https://doi.org/10.1021/es4053413.
[75] N.S. Grac, S. Pais, V.M.T.M. Silva, E. Rodrigues, Oxygenated Biofuels from Butanol for Diesel Blends : Synthesis of the Acetal 1 , 1-Dibutoxyethane Catalyzed by Amberlyst-15 Ion-Exchange Resin, 2010, pp. 6763–6771.
[76] J. Wu, D. Ren, X. Zhang, Z. Chen, S. Zhang, S. Li, L. Fu, The adsorption properties of biochar derived from woody plants or bamboo for cadmium in aqueous solution, Desalination Water Treat. 160 (2019) 268–275, https://doi.org/10.5004/dwt.2019.24174.
[77] M. Srinivas, G. Raveendra, G. Parameswaram, P.S.S. Prasad, N. Lingaiah, Journal of molecular catalysis A : Chemical cesium exchanged tungstophosphoric acid supported on tin oxide : an efficient solid acid catalyst for etherification of glycerol with tert -butanol to synthesize biofuel additives, J. Mol. Catal. Chem. 413 (2016) 7–14, https://doi.org/10.1016/j.molcata.2015.10.005.
[78] R. Huang, E.Y. Kim, Catalytic synthesis of glycerol tert-butyl ethers as fuel additives from the biodiesel by-product glycerol, J. Chem. 2015 (2015), https://doi.org/10.1155/2015/763854.
[79] R. Zhou, Y. Jiang, B. Ye, H. Zhao, Z. Hou, Synthesis of Jet Fuel from Glycerol and Tert -Butyl Alcohol Under Microwave Irradiation, (n.d.) 1–13.
[80] R. Estevez, S. Lopez-Pedrajas, D. Luna, F.M. Bautista, Microwave-assisted etherification of glycerol with tert-butyl alcohol over amorphous organosilica-aluminum phosphates, Appl. Catal., B 213 (2017) 42–52, https://doi.org/10.1016/j.apcatb.2017.05.007.
[81] M. Gonçalves, M. Mantovani, W. Alves, R. Rodrigues, D. Mandelli, J. Silvestre, Biodiesel Wastes : an Abundant and Promising Source for the Preparation of Acidic Catalysts for Utilization in Etherification Reaction, 256, 2014, pp. 468–474, https://doi.org/10.1016/j.cej.2014.07.013.
[82] W. Li, D. Wang, Y. Zhu, J. Chen, Y. Lu, S. Li, Y. Zheng, Z. Zheng, Efficient ex-situ catalytic upgrading of biomass pyrolysis vapors to produce methylfurans and phenol over bio-based activated carbon, Biomass Bioenergy 142 (2020), https://doi.org/10.1016/j.biombioe.2020.105794.
[83] R. Estevez, M.I. López, C. Jiménez-Sanchidrián, D. Luna, F.J. Romero-Salguero, F. M. Bautista, Etherification of glycerol with tert-butyl alcohol over sulfonated hybrid silicas, Appl. Catal. Gen. 526 (2016) 155–163, https://doi.org/10.1016/j.apcata.2016.08.019.
[84] H. Shafiei, A. Khonsari, P. Mousavi, Serverless Computing: a Survey of Opportunities, Challenges, and Applications, 54, ACM Comput Surv, 2022, https://doi.org/10.1145/3510611.